

Article

Facile Synthesis of Copper(I) Oxide Nanochains and the Photo-Thermal Conversion Performance of Its Nanofluids

Zhongjin Ni ¹, Xiaohai Cao ², Xinyi Wang ¹, Shiyu Zhou ¹, Caixia Zhang ², Bin Xu ^{2,*} and Yihua Ni ^{1,*}

¹ College of Engineering, Zhejiang A&F University, Lin'an 311300, China; neezj@zafu.edu.cn (Z.N.); wangxinyi9219@sina.com (X.W.); shiyuzhou98@sina.com (S.Z.)

² College of Materials Science and Engineering, Zhejiang University of Technology, Hangzhou 310014, China; xiaohaicao_zjut@sina.com (X.C.); caixiazhang_zjut@sina.com (C.Z.)

* Correspondence: xub@zjut.edu.cn (B.X.); 20120006@zafu.edu.cn (Y.N.)

Abstract: In this thesis, Cu₂O nanochains were synthesized by thermal decomposition with copper formate-octylamine as the precursor, oleic acid and oleylamine as the catalyst stabilizer agent and paraffin as the solvent. The phase structure and micromorphology of Cu₂O nanochains were characterized by X-ray diffraction and transmission electron microscopy. The effect of reaction time and concentration of the precursor on the Cu₂O nanochains were discussed, and the formation mechanism of the Cu₂O nanochains was analyzed. The results show that Cu₂O nanochains were self-assembled by Cu₂O nanocrystals; with the extension of the reaction time, Cu₂O nanochains gradually become granular; increasing the concentration of the precursor will increase the entanglement degree of the nanochains. Oleic acid contributes to the formation of Cu₂O, and oleylamine plays a directional role in the formation of nanochains. On the basis of those phenomenon, a comparison of the Cu₂O nanochain-water nanofluids with that of a water-based liquid showed that after irradiating for 3000 s, the temperature of nanofluids reached 91.1 °C while the water was only 75.7 °C. This demonstrates the better performance of the Cu₂O nanochain-water nanofluid in the ability of light absorption, thermal conductivity and photothermal conversion.

Keywords: cuprous oxide nanochains; thermal decomposition; nanofluids; photo-thermal conversion performance



Citation: Ni, Z.; Cao, X.; Wang, X.; Zhou, S.; Zhang, C.; Xu, B.; Ni, Y.

Facile Synthesis of Copper(I) Oxide Nanochains and the Photo-Thermal

Conversion Performance of Its Nanofluids. *Coatings* **2021**, *11*, 749.

<https://doi.org/10.3390/coatings11070749>

Academic Editor: Ivan Jerman

Received: 21 May 2021

Accepted: 17 June 2021

Published: 22 June 2021

Publisher's Note: MDPI stays neutral with regard to jurisdictional claims in published maps and institutional affiliations.



Copyright: © 2021 by the authors. Licensee MDPI, Basel, Switzerland. This article is an open access article distributed under the terms and conditions of the Creative Commons Attribution (CC BY) license (<https://creativecommons.org/licenses/by/4.0/>).

1. Introduction

Solar thermal utilization is a technology that can utilize the sun's radiation efficiently. Meanwhile, the solar collector is a device that can be used to absorb the sun's radiation and convert it into thermal energy, then the thermal energy is transferred to the heat transfer medium. Currently, all of the traditional flat plate and vacuum tube collectors are almost using indirect heat collection. After the solar radiation is absorbed by selective coating and converted into thermal energy, only by going through the thermal conductivity process of the coated metal plate or glass tube wall can the thermal energy be transferred to the working fluid. Therefore, with the increasing surface temperature of the heat collector, the radiation heat loss from the high-temperature surface to the environment is increasing as well, consequently, the conversion efficiency will be reduced. In the 1975s, Minardi proposed a conception about direct absorption solar collectors (DASC) in order to reduce the high-temperature radiant heat loss and improve the thermal efficiency [1]. Different from the indirect heat collector, this kind of solar heat collector does not have a heat-absorbing surface and the solar radiation will be absorbed directly by the working fluid so it can reduce the radiant heat loss and avoid the conducted thermal resistance between the endothermic surface and the working fluid. However, the working fluid for the DASC has usually been a kind of black liquid which is prepared by adding black ink, black dye and other common micron particles into the medium, such as water or ethylene glycol. However, this black liquid has some defects such as instability of the light,

heat-induced degradation, ease clogging and low thermal conductivity. Therefore, the DASC based on the black liquid can not achieve the desired high efficiency and obstructed the development and application of this kind of new type collector. With the development of nanotechnology and the application of nanomaterial, in 1995, Choi et al. proposed a concept called “Nanofluids” in the international community for the first time, which is a kind of liquid adding nanoscale metal and non-metallic oxide particles in a certain manner and ratio, which will form a new class of heat transfer medium [2]. Soon after, numerous researches for the thermal physical properties, enhancing heat transfer performance et al. of the nanofluids have been performed by scientists; the results indicated that nanofluids have significant heat transfer performance [3,4]. The binary CuO/ZnO nanofluids were prepared and the thermal conductivity, as well as the photothermal conversion, were investigated by Fang [5]. The optical absorption properties and the thermal conductivity were both enhanced due to the presence of the CuO/ZnO nanoparticles in the nanofluids.

In the meantime, with the existence of nanoparticles, the absorption, transmission, and scattering of solar radiation by nanofluids has changed and its optical properties are different from the common fluids which mean light can be strongly absorbed or selectively absorbed by the nanofluids at some bands in solar radiation [6]. In view of the special light absorption performance and the good heat transport performance of nanofluids, in recent years, some scholars proposed that in order to enhance the efficiency of the heat collector, nanofluids can be used as the working medium for the DASC, which can absorb the sun’s radiation energy directly. It can be demonstrated from the research results that the efficiency of heat collection for DASC based on the nanofluids had obviously been enhanced [7–9]. It showed that nanofluids have a large application potential as the working media for DASC.

Cuprous oxide nanoparticles are known as a kind of typical p-type semiconductor with a bandgap of 2.0–2.3 eV [10], which has a high absorption coefficient for visible light. On account of its excellent electrical [11] and magnetic properties [12], Cu₂O has become a hot research topic in the field of optoelectronics, catalysis and diluted magnetic semiconductors (DMSs). It is an important material to manufacture low-cost solar cell and gas sensors. However, there are two factors impeding its development in the field of photoelectrochemistry. One is the inconsistency between the diffusion length and the absorption depth of the light near the bandgap of Cu₂O intrinsic carrier [13–15], and the other one is the instability [16–18] of optical absorption of Cu₂O in solution. The Cu₂O has a huge surface and a high aspect ratio, and it can collect and separate the effect carrier from the radial in the nanometer scale while it is absorbing the light along the long axis, so it has a higher ability of light absorption than the Cu₂O nanoparticles [19]. Additionally, the chain (liner) structure of the Cu₂O nanochains makes it easier to form the thermal network chain, which can improve the thermal conductivity of the nanofluids, thereby its heat transfer efficiency will be improved.

The nanoparticles tend to agglomerate in the base fluid due to the effect of the Van der Waals force and hydrogen bonding. During the experiment to determine the thermal conductivity of Fe₃O₄-water nanofluids by Zhu [20], they found that the nanoparticles had been aligned to nanochains caused by the agglomeration accidentally. The number and length of alignments increase with the increase in the nanoparticle’s concentration, leading to the sharp increases of the thermal conductivities. The results are consistent with the simulation results of the effective thermal conductivity of fluid-particle mixture by Kumar and Murthy [21]. The enhancement from the nanochains to the nanofluids can be explained from two sides.

First, the single nanochains have a thermal conductivity enhancement compared to the single nanoparticles. The heat transfer process in the nanochains is a non-Fourier phenomenon, therefore the thermal conductivity changes with the shape and the size of the materials. According to the result from the experiment about the thermal conductivity of monatomic nanochains by Chen [22], an atomic nanochain can be thought of as a finite one-dimensional lattice in which lattice vibrational waves must be reflected at the ends.

The transmission direction of the energy will be changed as well so that the energy flux will be reduced as will the thermal conductivity. The shorter the nanochains are, the smaller the attenuation of a lattice vibration wave will be before it reaches the end. The whole energy flux will reduce which will result in the reduction of the thermal conductivity.

The result demonstrates the relationship between the length of the nanochains and the thermal conductivity from the microscope point with the view of phonon and lattice wave transmission. On the other side, Moran et al. compared the conduction of heat in the nanochains to the flow of gas in the nanochannels by theoretical analysis and molecular dynamics (MD) simulation from the macroscope point when studying the thermal conductivity of silicon nanochains [23]. The thermal resistance caused by the end effect in this way of heat transfer was:

$$f_T = \frac{2\gamma\rho C^2 T}{c^2 k(1 - e^{-D/l})e^{-ND/l} q} \quad (1)$$

where q is the heat flux, T the local thermodynamic equilibrium temperature, ρ the solid density, C the solid specific heat capacity, γ the Grüneisen constant, l the length of nanochain and N can be understood as the dimensionless length of ends effect region normalized by the channel width. For a straight channel, an empirical value of N is 5. From this formula, the heat resistance caused by the end effect will be negligible when the length of nanochain is long enough. That is, the thermal conductivity will be improved when the length of nanochain increases.

Secondly, the synergistic effect among the nanochains in the nanofluids will also lead to the enhancement of the thermal conductivity of nanofluids. Figure 1a shows the network structure formed by the bridge-like overlap of the nanochains which are parallel to the direction of the heat transfer and the randomly aligned nanochains in the nanofluids. This phenomenon of bridge-like overlap is mainly caused by the high ratio aspect of the nanochains. These networks provide a low-resistance pathway to heat conduction and increase the overall thermal conductivity of the composite. Compared to the nanochains, the nanoparticles are unable to join to form an effective thermal conduction path in the nanofluid, shown in Figure 1b. So the thermal conductivity of the nanofluids with nanoparticles will be lower than that of the nanochains [24].

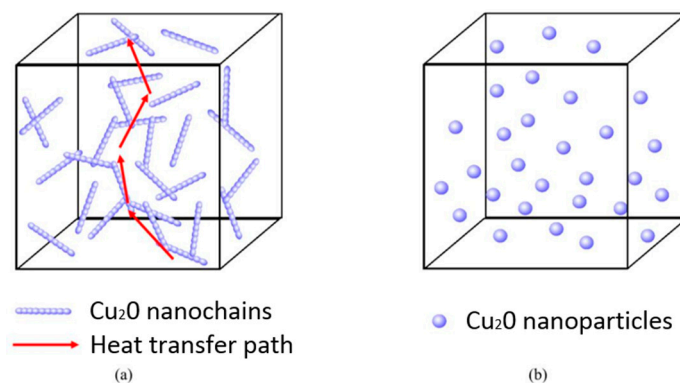


Figure 1. Schematics diagram of the heat transfer process of (a) Cu_2O nanochains and (b) Cu_2O nanoparticles in the nanofluids.

Due to the large specific surface area and high aspect ratio, Cu_2O nanochains can absorb light along the long axis and the effective carrier collection and separation can be carried out at the same time in the nanometer scale [25], which is expected to solve the problem above. However, the research about the photo-thermal conversion performance of Cu_2O nanochains-water nanofluids has been barely developed by now. In this paper, the innovative mixing of Cu_2O nanochains with water as the working media can prepare nanofluids to improve the heat collection efficiency of DASC with the photothermal con-

version properties it possesses. Cu_2O nanochains are mainly synthesized by the template method [26] and the chemical reduction method [27], both of which have relatively obvious disadvantages. It is difficult to separate using the template method, and the chemical reduction method depends on the environmentally unfriendly reductant. Here we report a method to facile synthesis of the Cu_2O nanochains, and several types of research about the formation mechanism of Cu_2O nanochains and the optical performance of Cu_2O nanochains-water nanofluids was performed. Section 2 details the preparation process and characterisation scheme of Cu_2O nanochains and their nanofluids. Section 3 analyses and discusses the influencing factors and formation mechanism of Cu_2O nanochains and the properties of Cu_2O nanofluids. Section 4 summarises the experimental results.

2. Materials and Methods

2.1. Materials and Reagents

Copper(II) formate tetrahydrate (AR) was purchased from Guanghua Sci-Tech Co., Ltd. Octylamine (AR, alladin, Shanghai, China); Efficient sliced paraffin (melting point 60~62 °C) was purchased from Shanghai Hualing Rehabilitation Equipment Company, (Shanghai, China); Oleic acid (CP) was purchased from Hangzhou Shuanglin Chemical Reagent Company(Hangzhou, China); Oleylamine (AR, alladin); n-hexane (AR) was purchased from Yonghua Fine Chemistry Co., Ltd. (Suzhou, China).

2.2. Synthesis

The synthesis process of Cu_2O nanochains is shown in Figure 2. Copper(II) formate tetrahydrate and octylamine were mixed with a mole ratio of 1:2. After stirring for 1 h at 35.0 °C, the precursor (the coordination complex of copper formate and octylamine) was prepared. The precursor (0.02 mol) was added to paraffin (6 g) with oleic acid (0.005 mol) and oleylamine (0.02 mol) stirring for 1 h at 70 °C, the mixture was added to the 50 mL flask with three necks with 6 g of the melted paraffin. After the addition process, the reaction mixture was heated to 130 °C in a temperature-controlled oil bath. A constant amount of nitrogen is introduced into the three-necked flask to ensure that the reaction apparatus is airtight and free of gas leaks. The precursor began to decompose under a constant stream of nitrogen and the color of the solution turned to dark brown from light blue. After heating for 1 h, the resulting products were centrifugally washed by n-hexane 3~4 times. Finally, the target products were obtained.

2.3. Characterization

The micro morphology of the Cu_2O nanochains was characterized by Tecnai G2 F30 Transmission electron microscope; the phase analysis was determined by using X'PERT PROX shooting line diffractometer over the scan range from 10° to 80° at a rate of 5°/min, using a copper target as the diffraction source ($\text{Cu K}\alpha$, $\lambda = 0.15406$ nm); the light absorption performance of the samples was determined by Lamda 750 s UV-visible-near-infrared spectrophotometer with the wavelength from 380 to 800 nm; the laboratory self-assembled light-heat conversion tester (Figure 3) was used to analyze the optical thermal conversion performance of the nanofluids which is prepared by spreading 4.8 wt.% Cu_2O nanochains into deionized water and going through the CTAB and ultrasonic process; Thermal conductivity of the suspension was determined by TC-3000 thermal conductivity meter in the temperature range from 30 to 80 °C at intervals of 10 °C, and the temperature was measured repeatedly and averaged for 10 times. The thermal conductivity enhancement ratio of nanofluids was calculated by the following equation:

$$E = (K_1 - K_0)/K_0 \quad (2)$$

where E is the thermal conductivity enhancement ratio; K_1 is the thermal conductivity of nanofluids, $\text{W}\cdot\text{m}^{-1}\cdot\text{K}^{-1}$; K_0 is the thermal conductivity of water, $\text{W}\cdot\text{m}^{-1}\cdot\text{K}^{-1}$.

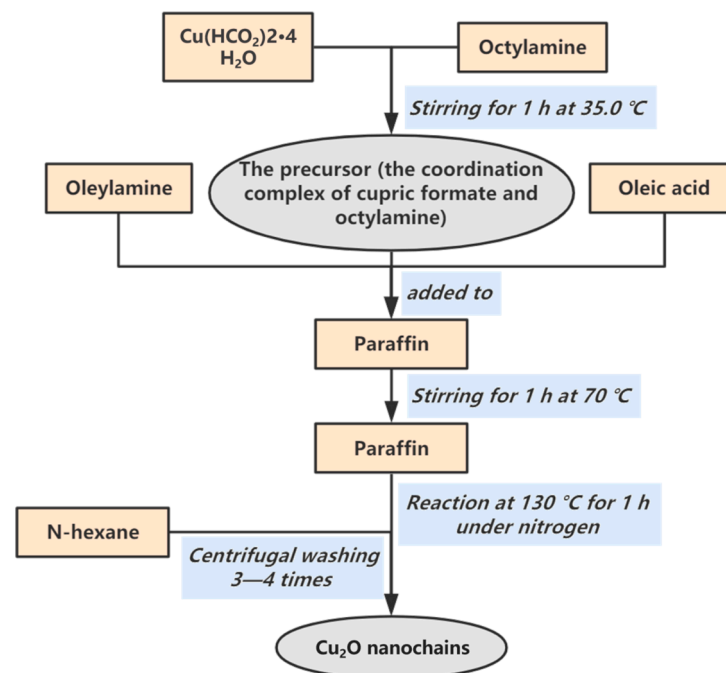


Figure 2. Synthesis process flow chart of Cu_2O nanochains.

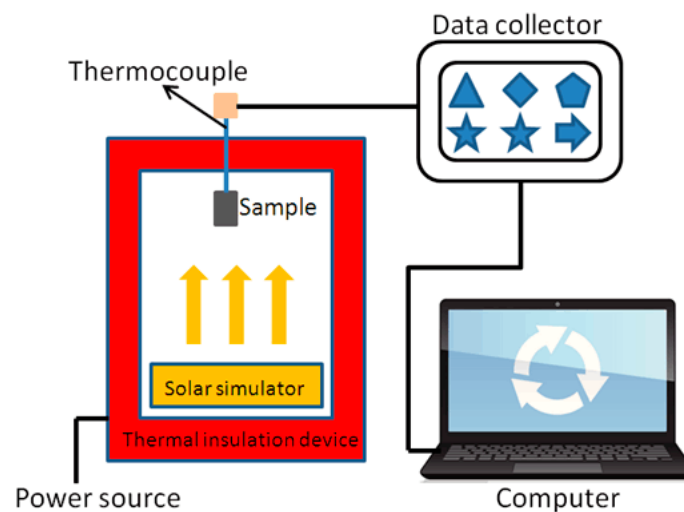


Figure 3. The apparatus for evaluating the light-thermal conversion performance [28].

3. Results and Discussion

3.1. The Characterization of Cu_2O Nanochains

Figures 4 and 5 show the XRD images and TEM images of Cu_2O nanochains, respectively. In the XRD pattern (Figure 4), the diffraction peaks are consistent with standard diffraction data of Cu_2O (No. JCPDF 040836). The diffraction peaks at 2θ values of 36.50° , 42.50° , 61.33° and 74.09° are corresponding to the diffractions of (111), (200) and (311) crystal planes of Cu_2O , respectively. The diffraction peaks are very sharp, which indicates the good crystallinity of the microcrystals. There are no other peaks that can be observed, implying that the nanochains prepared by thermal decomposition have high purity.

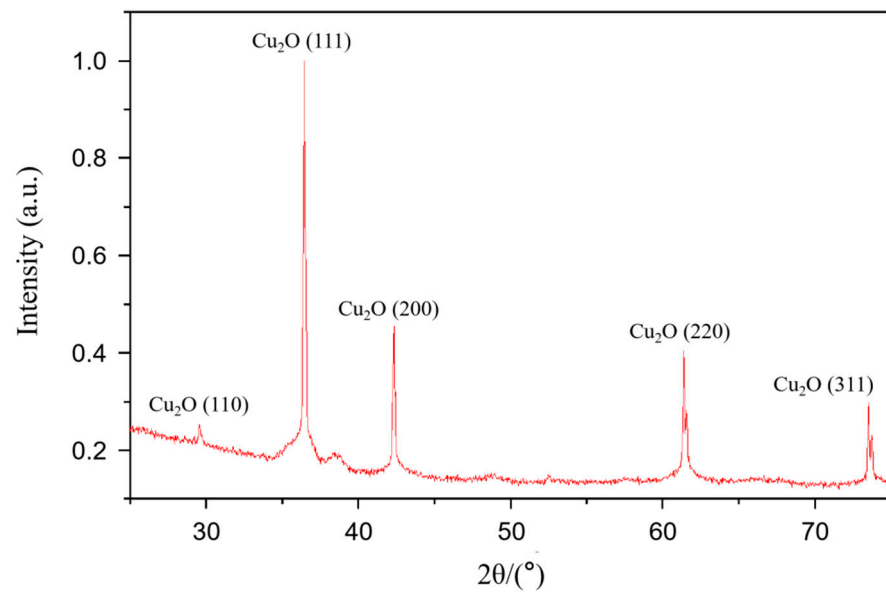


Figure 4. XRD pattern of Cu_2O nanochains.

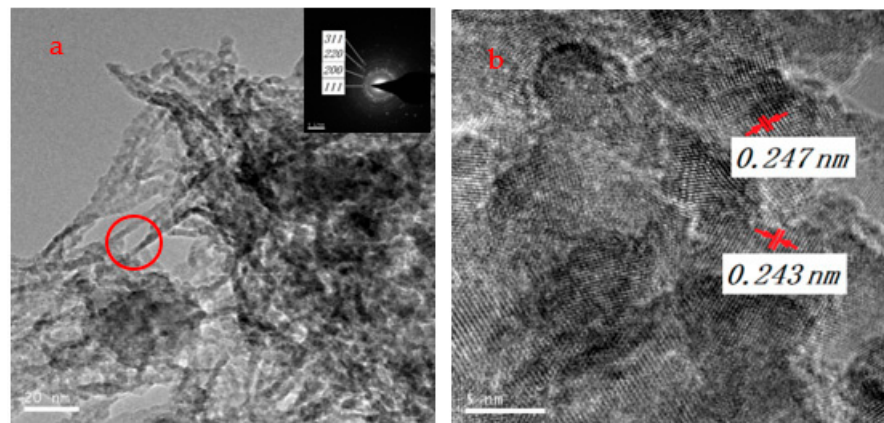


Figure 5. TEM photos of Cu_2O nanochains and (b) is an enlarged view of the red zone of (a).

The morphology of the nanofluids by TEM is presented in Figure 5. A large number of entangled nanochains can be observed in the TEM image shown in Figure 5a, the diameter is about 2~3 nm. The selected area electron diffraction (SAED) of the upper right corner of Figure 5a shows the multi-crystal diffraction ring, it is corresponding to the (111), (200) and (220) crystal planes of Cu_2O from the inner space to the outside in turn. The different lattice fringe directions in this picture indicate that there are many Cu_2O micro-crystallizes with different sizes, and Cu_2O nanochains are composed of a large number of Cu_2O micro-crystallizes by self-assembly.

3.2. The Effect Factors of the Formation of Cu_2O Nanochains

3.2.1. The Effect of Reaction Time on the Morphology of the Product

In order to study the effect of reaction time on the morphology of the product, we set the time to 0.5 and 2 h and keep the other parameters constant. The morphology of the product is shown in Figure 6. When the reaction time is 0.5 h, the products are small particles with a diameter of about 10 nm (shown in Figure 6a); when the reaction time prolonged from 0.5 h to 1 h, the nanochains appeared (shown in Figure 5); when the reaction time reached 2 h, the diameter of larger particles with whiskers around the surface is about 100 nm (shown in Figure 6b). That is due to the particles entering the intraparticle ripening stage with the extension of the reaction time during the growing of nano-crystallizes. In the reaction system where the Cu_2O was prepared, the precursor

produces plenty of molecules of Cu_2O by thermal decomposition; these molecules nucleate and polymerize into nanocrystalline and then self-assemble into nanochains within a short time period. Afterward, the concentration of Cu_2O decreases rapidly and the Cu_2O nanochains will enter the Ostwald ripening stage [29]. The small particles with larger solubility tend to be dissolved, and the monomers will recrystallize on the surface of larger particles. These phenomena all follow the Ostwald ripening mechanism. Ostwald ripening is a phenomenon that can be observed in solid or liquid solutes and describes the change of a non-uniform structure with the passage of time: smaller crystalline or solute particles in the solute dissolve and are deposited again on larger crystalline or solute particles. Consequently, when the Cu_2O nanochains appear in the reaction system, the low concentration of Cu_2O results in the dissolving of nano-crystallizes progressively, and the larger particles of Cu_2O will grow on by adsorbing the small particles of Cu_2O . Finally, a large crystal of Cu_2O is obtained.

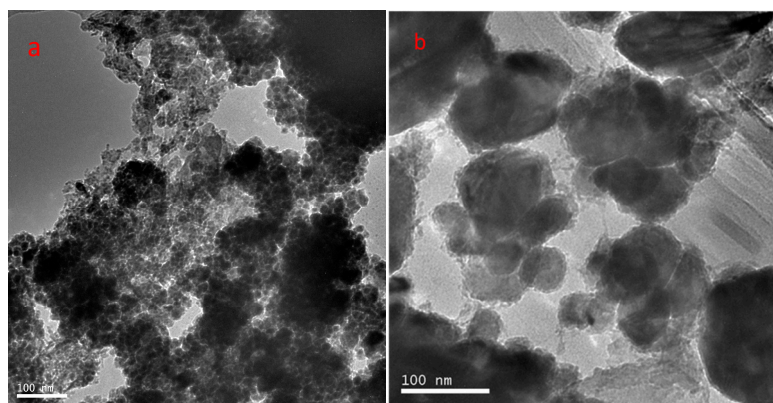


Figure 6. TEM photos of the products with different reaction times (a) 0.5 h; (b) 2 h.

3.2.2. The Effect of Precursor Concentration on the Morphology of the Product

In order to investigate the influence of precursor concentration on the morphology of the product, the precursor concentration was adjusted to 0.005 mol and 0.04 mol and keep the other parameters constant. The morphology of the resulting product is shown in Figure 7. It can be seen from the picture that when the precursor concentration is 0.005 mol, less Cu_2O is generated, the particle is mainly formed by nucleation, therefore the morphology of the final product is mainly small particles (Figure 7a), those small particles have connected together, the condition of forming chains was initially formed. With the increase in the concentration of the precursor to 0.04 mol, the number of nanochains increased, and the entanglement degree of the nanochains also increased (Figure 7b). In this paper, the Cu_2O nanochains reaction system is a homogeneous reaction system, and the nucleation process and growth process are all dependent on the supersaturation of Cu_2O , that is the difference between the solubility of Cu_2O concentration and Cu_2O nanoparticles [30]. When Cu_2O has a lower supersaturation, Cu_2O nanoparticles will grow faster than the nucleation, and it is conducive to the growth of Cu_2O nanoparticles; when Cu_2O supersaturation is higher, the nucleation of Cu_2O nanoparticles will be the dominant part in the growing process. Therefore, increasing the precursor concentration can increase the number of Cu_2O molecules, which also contributes to improving the supersaturation of the system. This will help the nucleation of Cu_2O nanoparticles to form more nanocrystals, which then self-assemble into Cu_2O nanochains. Consequently, too many Cu_2O nanochains lead to an increasing degree of entanglement.

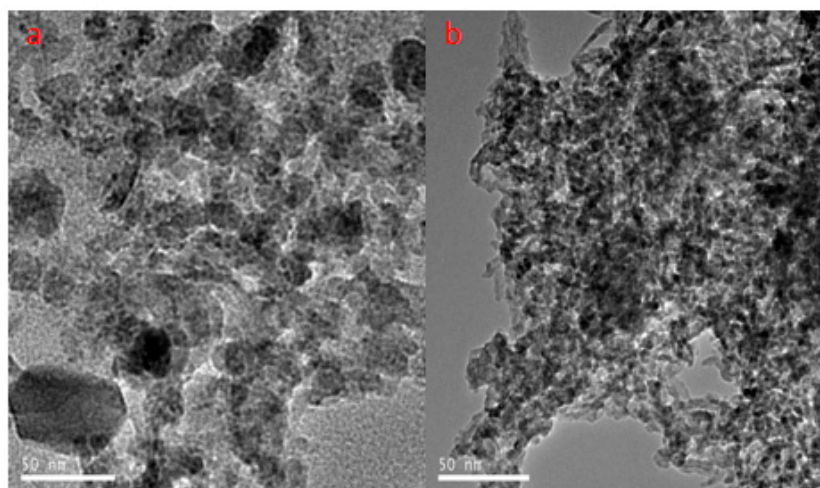


Figure 7. TEM photos of the products with different precursor concentration (a) 0.005 mol; (b) 0.04 mol.

3.3. The Formation Mechanism of Cu_2O Nanochains

The complexes made up of the copper formate and octylamine can increase its solubility in the paraffin, which can reduce the thermal decomposition temperature of copper formate, and inhibit the growth of the nanoparticles [31]. The addition of oleic acid is beneficial to the formation of Cu_2O by the final thermal decomposition of the complex. The formation mechanism of Cu_2O is that the coordination complex of copper formate and octylamine ($\text{Cu}(\text{HCOO})_2 \cdot 4\text{H}_2\text{O}$) can produce H_2O and $\text{Cu}(\text{HCOO})_2$ by thermal decomposition, for the water is surrounded by the liquid paraffin and forming a W/O structure in the liquid paraffin. $\text{Cu}(\text{HCOO})_2$ is a polar molecule, being dissolved in water can promote $\text{Cu}(\text{HCOO})_2$ partial ionization and producing Cu^{2+} and HCOO^- . Additionally, organic acid has reducibility [32], while HCOO^- does not have reducibility, when oleic acid is added into the reactant, due to the weak acidity of oleic acid, a small amount of hydrogen ions are captured by HCOO^- , resulting in the HCOO^- having reducibility. Therefore, in the presence of hydrogen ions, HCOO^- reduced the Cu^{2+} to Cu^+ , the reaction equation is as follows:



Cu^+ combined with H_2O to generate CuOH , CuOH is heated to generate Cu_2O and H_2O , the reaction equation is described as follows:



The total reaction equation as follows [33]:



The formation mechanism of Cu_2O nanochains is shown in Figure 8. Compared to the electron-based carboxyl group of oleic acid, the amino group of the oleylamine with a stronger nucleophilicity reacts with the copper atoms in Cu_2O more easily to compensate unbalance of the charge so that the surface of the crystal will be stabilized. The crystal plane of Cu_2O (111) contains an unsaturated dangling bond of copper, therefore it reacts easier with oleylamine and reduces the surface energy of the crystal plane (111) compared to that of the crystal plane (100) or (110) [34]. In addition, a clear steric hindrance, formed by the long carbon chain of oleylamine on the surface of the nanoparticles, increases the repulsion of the connection of the Cu_2O crystal plane (111). Therefore, a long-range order structure with high leak-proof ability is formed on the surface of Cu_2O covered by oleylamine, while the rest of the Cu_2O surface still is highly active [35]. The interacted Cu_2O nano-crystallizes

with special structure self-assemble into a thread and all the produced surfaces are crystal planes (111), as shown in Figure 8.

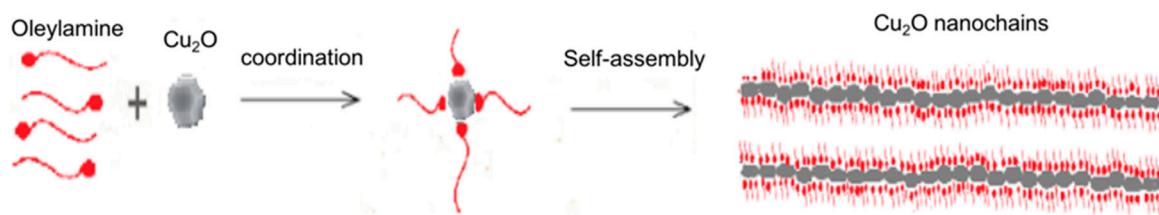


Figure 8. The schematic diagram of the formation mechanism of Cu_2O nanochains.

3.4. Thermo-Physical Properties and Photo-Thermal Performance of Nanofluids

Figure 9A shows the temperature-thermal conductivity curve of the Cu_2O nanochains-water nanofluids and water. It can be seen from the curve that the thermal conductivity of nanofluids is all higher than that of water. This is mainly due to the fact that the thermal conductivity of Cu_2O nanochains is much higher than that of the water, and there is the micro convection heat transfer caused by the irregular Brownian motion of the Cu_2O nanochains [36] inside the fluids in the meantime. The thermal conductivity of nanofluids increases from $0.6330 \text{ W}\cdot\text{m}^{-1}\cdot\text{K}^{-1}$ to $0.7137 \text{ W}\cdot\text{m}^{-1}\cdot\text{K}^{-1}$ as the temperature increases from 30 to 80 °C, that is, the thermal conductivity increases almost linearly, which is consistent with the results of Zamzaman et al. [37]. As is shown in Figure 9B, the thermal conductivity enhancement ratio of nanofluids was 3.16% at 30 °C. When the temperature is raised to 80 °C, the thermal conductivity enhancement ratio of nanofluids reaches 6.68%. The enhancement of the thermal conductivity is mainly due to the fact that the viscosity of the nanofluids decreases as the temperature is raised up, with the irregular Brownian motion increases, so that the micro-convection heat transfer inside the fluids will be enhanced [38–41].

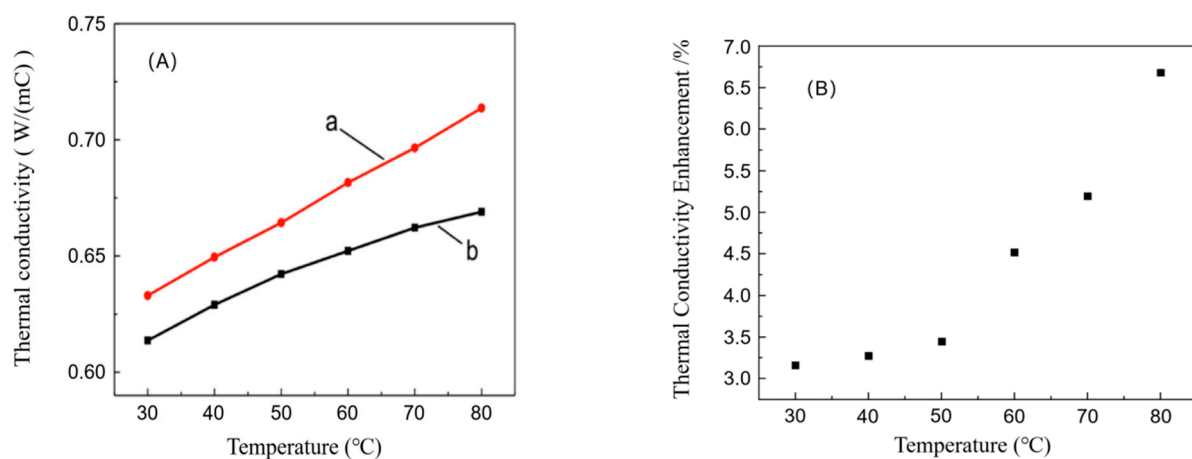


Figure 9. (A): The photographs of temperature-thermal conductivity curve of water (a) and nanofluids (b); (B): Thermal conductivity enhancement ratio of nanofluids in the different temperatures.

As is shown in this spectrum of nanofluids, the light absorption performance of nanofluids is obviously better than that of water. Attributes to the high ability of light absorption which the nanochains possessed, the addition of the nanochains will be able to enhance the light absorption capacity of nanofluids significantly (Figure 10).

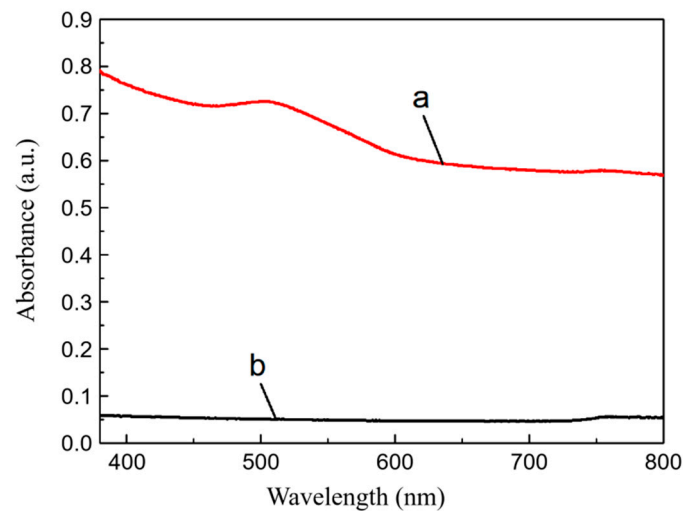


Figure 10. UV-vis pattern of water (a) and Cu_2O nanochains-water nanofluids (b).

Figure 11 shows the time-temperature curve of Cu_2O nanochains-water nanofluids and water under the irradiation of a self-made analog light source. From these pictures, we can figure out that both curves are in a monotonous upward trend while the rate of rising is both decreasing under the irradiation of the same light intensity ($1000 \text{ W}\cdot\text{m}^{-2}$). Additionally, the temperature of nanofluids was always higher than that of water. After irradiating for 3000 s, the temperature of nanofluids reached $91.1 \text{ }^\circ\text{C}$ while the water was only $75.7 \text{ }^\circ\text{C}$. Obviously, the photothermal conversion performance of Cu_2O nanochains-water nanofluids was enhanced significantly compared to that of water. That is mainly due to the fact that the solar spectral absorption characteristics have changed and the scattering and the absorption of light have been enhanced when Cu_2O nanochains are added into the water. The above results show that the Cu_2O nanochains-water nanofluids possess significant thermal-physical and photo-thermal conversion performance, and they can be the heat transfer medium for DASC.

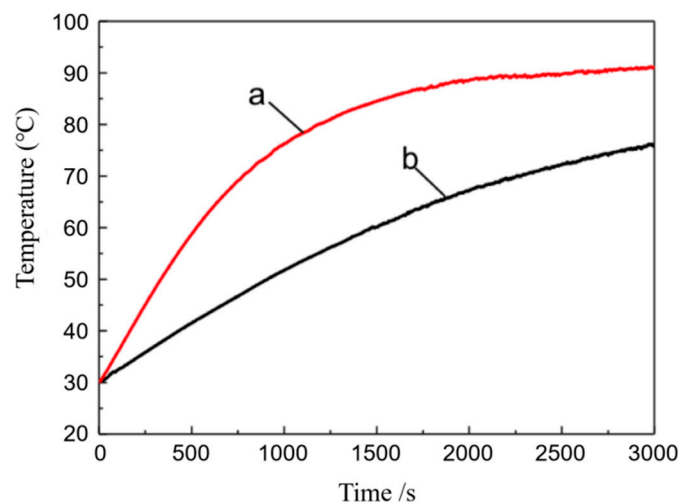


Figure 11. The time-temperature curve of water (a) and Cu_2O nanochains-water nanofluids (b) under the irradiation of self-made analog light source.

4. Conclusions

In melted paraffin, the Cu_2O nanochains (2–3 nm in diameter), self-assembled from Cu_2O nanocrystals, are prepared by thermal decomposition of a precursor with coordination compound with copper formate tetrahydrate and octylamine. Cu_2O nanochains become granular gradually as reaction time prolongs. The increasing concentration of the precursor

accelerates the agglomeration of the nanochains. Oleic acid is conducive to form Cu_2O , while oleylamine plays a directional role in forming the nanochains. The comparison between the Cu_2O nanochains, water nanofluids and the water base fluids shows that the former has better light absorption ability, thermal conductivity and photo-thermal conversion ability, which makes it qualify as a heat transfer medium for DASC. Future research can be conducted in several ways. Firstly, the composition of the nanochains in nanofluids can have a significant impact on the performance of nanofluids, and therefore research into optimal nanochain materials is one of the priorities for future research. Secondly, previous experiments have demonstrated that there is a correlation between nanofluids efficiency and concentration, but an increase in nanofluids concentration leads to an increase in viscosity, which affects the nanofluids efficiency. Therefore, an optimal concentration range may exist. In addition, previous studies have not considered the correlation between the properties of nanofluids and the size of the nanostrands within it, so this may also be a direction of interest for future research.

Author Contributions: Conceptualization and writing—original draft preparation, Z.N.; data collection and data analysis, X.C.; data interpretation, X.W.; literature search, S.Z.; data collection, C.Z.; study design and writing, B.X.; study design, Y.N. All authors have read and agreed to the published version of the manuscript.

Funding: This research was funded by the Planning Project of Application Research for Public Service Technology of Zhejiang Province (LGG18E060002) and Zhejiang Provincial Collaborative Innovation Center for Bamboo Resources and High-efficiency Utilization (2017ZZY2-15).

Institutional Review Board Statement: Not applicable.

Informed Consent Statement: Informed consent was obtained from all subjects involved in the study.

Data Availability Statement: The data used to support the findings of this study are obtained directly from the simulation by the authors.

Conflicts of Interest: The authors declare no conflict of interest.

References

1. Goel, N.; Taylor, R.A.; Otanicar, T. A review of nanofluid-based direct absorption solar collectors: Design considerations and experiments with hybrid PV/Thermal and direct steam generation collectors. *Renew. Energy* **2020**, *145*, 903–913. [[CrossRef](#)]
2. Wang, K.; He, Y.; Liu, P.; Kan, A.; Yu, W. Highly-efficient nanofluid-based direct absorption solar collector enhanced by re-verse-irradiation for medium temperature applications. *Renew. Energy* **2020**, *159*, 652–662. [[CrossRef](#)]
3. Hong, S.W.; Kang, Y.-T.; Kleinstreuer, C.; Koo, J. Impact analysis of natural convection on thermal conductivity measurements of nanofluids using the transient hot-wire method. *Int. J. Heat Mass Transf.* **2011**, *54*, 3448–3456. [[CrossRef](#)]
4. Saidur, R.; Leong, K.; Mohammed, H. A review on applications and challenges of nanofluids. *Renew. Sustain. Energy Rev.* **2011**, *15*, 1646–1668. [[CrossRef](#)]
5. Fang, J.; Xuan, Y. Investigation of optical absorption and photothermal conversion characteristics of binary CuO/ZnO nanofluids. *RSC Adv.* **2017**, *7*, 56023–56033. [[CrossRef](#)]
6. Lenert, A.; Wang, E.N. Optimization of nanofluid volumetric receivers for solar thermal energy conversion. *Sol. Energy* **2012**, *86*, 253–265. [[CrossRef](#)]
7. Otanicar, T.P.; Phelan, P.E.; Prasher, R.S.; Rosengarten, G.; Taylor, R.A. Nanofluid-based direct absorption solar collector. *J. Renew. Sustain. Energy* **2010**, *2*, 033102. [[CrossRef](#)]
8. Saidur, R.; Meng, T.C.; Said, Z.; Hasanuzzaman, M.; Kamyar, A. Evaluation of the effect of nanofluid-based absorbers on direct solar collector. *Int. J. Heat Mass Transf.* **2012**, *55*, 5899–5907. [[CrossRef](#)]
9. Tyagi, H.; Phelan, P.; Prasher, R. Predicted Efficiency of a Low-Temperature Nanofluid-Based Direct Absorption Solar Collector. *J. Sol. Energy Eng.* **2009**, *131*, 143–155. [[CrossRef](#)]
10. Xu, B.; Chen, C.; Zhou, J.; Ni, Z.; Ma, X. Preparation of novel microencapsulated phase change material with $\text{Cu-Cu}_2\text{O}/\text{CNTs}$ as the shell and their dispersed slurry for direct absorption solar collectors. *Sol. Energy Mater. Sol. Cells* **2019**, *200*, 109980. [[CrossRef](#)]
11. Dai, P.; Li, W.; Xie, J.; He, Y.; Thorne, J.; McMahon, G.; Zhan, J.; Wang, D. Forming buried junctions to enhance the photovoltage generated by cuprous oxide in aqueous solutions. *Angew. Chem. Int. Ed.* **2014**, *53*, 13493–13497. [[CrossRef](#)]
12. Wang, J.; Ma, J.; Li, X.; Li, Y.; Zhang, G.; Zhang, F.; Fan, X. Cu_2O mesoporous spheres with a high internal diffusion capacity and improved catalytic ability for the aza-Henry reaction driven by visible light. *Chem. Commun.* **2014**, *50*, 14237–14240. [[CrossRef](#)] [[PubMed](#)]

13. Shah, J.; Kumar, S.; Ranjan, M.; Sonvane, Y.; Thareja, P.; Gupta, S.K. The effect of filler geometry on thermo-optical and rheo-logical properties of CuO nanofluid. *J. Mol. Liq.* **2018**, *272*, 668–675. [[CrossRef](#)]
14. Hacialioglu, S.; Meng, F.; Jin, S. Facile and mild solution synthesis of Cu₂O nanochains and nanotubes driven by screw dislocations. *Caryologia* **2012**, *31*, 449–456.
15. Zhao, L.; Dong, W.; Zheng, F.; Fang, L.; Shen, M. Interrupted growth and photoelectrochemistry of Cu₂O and Cu particles on TiO₂. *Electrochim. Acta* **2012**, *80*, 354–361. [[CrossRef](#)]
16. Zhang, D. Synergetic effects of Cu₂O photocatalyst with titania and enhanced photoactivity under visible irradiation. *Acta Chim. Slovaca* **2013**, *6*, 141–149. [[CrossRef](#)]
17. Tran, P.D.; Batabyal, S.K.; Pramana, S.S.; Barber, J.; Wong, L.H.; Loo, S.C. A cuprous oxide-reduced graphene oxide (Cu₂O-rGO) composite photocatalyst for hydrogen generation: Employing rGO as an electron acceptor to enhance the photocatalytic activity and stability of Cu₂O. *Nanoscale* **2012**, *4*, 3875–3878. [[CrossRef](#)] [[PubMed](#)]
18. Zhang, Z.; Dua, R.; Zhang, L.; Zhu, H.; Zhang, H.; Wang, P. Carbon-layer-protected cuprous oxide nanowire arrays for efficient water reduction. *ACS Nano* **2013**, *7*, 1709–1717. [[CrossRef](#)] [[PubMed](#)]
19. Zhao, Y.; Wang, W.; Li, Y.; Zhang, Y.; Yan, Z.; Huo, Z. Hierarchical branched Cu₂O nanochains with enhanced photocatalytic activity and stability for H₂ production. *Nanoscale* **2014**, *6*, 195–198. [[CrossRef](#)]
20. Zhu, H.; Zhang, C.; Liu, S.; Tang, Y.; Yin, Y. Effects of nanoparticle clustering and alignment on thermal conductivities of Fe₃O₄ aqueous nanofluids. *Appl. Phys. Lett.* **2006**, *89*, 023123. [[CrossRef](#)]
21. Zeiny, A.; Jin, H.; Bai, L.; Lin, G.; Wen, D. A comparative study of direct absorption nanofluids for solar thermal applications. *Sol. Energy* **2018**, *161*, 74–82. [[CrossRef](#)]
22. Chen, W.; Zou, C.; Li, X. An investigation into the thermophysical and optical properties of SiC/ionic liquid nanofluid for direct absorption solar collector. *Sol. Energy Mater. Sol. Cells* **2017**, *163*, 157–163. [[CrossRef](#)]
23. Wang, M.; Shan, X.; Yang, N. Understanding length dependences of effective thermal conductivity of nanochains. *Phys. Lett. A* **2012**, *376*, 3514–3517. [[CrossRef](#)]
24. Zhu, D.H.; Yu, W.; Du, H.X.; Chen, L.F.; Li, Y.; Xie, H.Q. Thermal conductivity of composite materials containing copper nanochains. *J. Nanomater.* **2016**, *2016*, 3089716. [[CrossRef](#)]
25. Hochbaum, A.; Yang, P. Semiconductor nanowires for energy conversion. *Chem. Rev.* **2010**, *110*, 527–546. [[CrossRef](#)] [[PubMed](#)]
26. Elisa, S.; Vallejo, J.P.; David, C.; Luis, L. Functionalized graphene nanoplatelet-nanofluids for solar thermal collectors. *Sol. Energy Mater. Sol. Cells* **2018**, *185*, 205–209.
27. Xu, B.; Zhou, J.; Ni, Z.; Zhang, C.; Lu, C. Synthesis of novel microencapsulated phase change materials with copper and copper oxide for solar energy storage and photo-thermal conversion. *Sol. Energy Mater. Sol. Cells* **2018**, *179*, 87–94. [[CrossRef](#)]
28. Xia, H.; Zinke-Allmang, M. Rate equation approach to the late stages of cluster ripening. *Phys. A Stat. Mech. Appl.* **1998**, *261*, 176–187. [[CrossRef](#)]
29. LaMer, V.K.; Dinegar, R.H. Theory, Production and mechanism of formation of monodispersed hydrosols. *J. Am. Chem. Soc.* **1950**, *72*, 4847–4854. [[CrossRef](#)]
30. Yabuki, A.; Tanaka, S. Electrically conductive copper film prepared at low temperature by thermal decomposition of copper amine complexes with various amines. *Mater. Res. Bull.* **2012**, *47*, 4107–4111. [[CrossRef](#)]
31. Chen, Z.-Z.; Shi, E.-W.; Zheng, Y.-Q.; Li, W.-J.; Xiao, B.; Zhuang, J.-Y. Growth of hex-pod-like Cu₂O whisker under hydrothermal conditions. *J. Cryst. Growth* **2003**, *249*, 294–300. [[CrossRef](#)]
32. Galwey, A.K.; Jamieson, D.; Brown, M.E. Thermal decomposition of three crystalline modifications of anhydrous copper(II) formate. *J. Phys. Chem.* **1974**, *78*, 2664–2670. [[CrossRef](#)]
33. Behura, A.K.; Gupta, H.K. Efficient direct absorption solar collector using nanomaterial suspended heat transfer fluid. *Mater. Today Proc.* **2020**, *22*, 1664–1668. [[CrossRef](#)]
34. Zeng, J.; Xuan, Y. Tunable full-spectrum photo-thermal conversion features of magnetic-plasmonic Fe₃O₄/TiN nanofluid. *Nano Energy* **2018**, *51*, 754–763. [[CrossRef](#)]
35. Fang, X.P. *Research on Heat and Mass Transfer Mechanisms and Optical Character of Nanofluids*; Nanjing University of Science and Technology: Nanjing, China, 2013.
36. Tajik Jamal-Abad, M. Thermal conductivity of Cu and Al-Water nanofluids. *Int. J. Eng.* **2013**, *26*, 821–828.
37. Sadri, R.; Ahmadi, G.; Togun, H.; Dahari, M.; Kazi, S.N.; Sadeghinezhad, E.; Zubir, N. An experimental study on thermal conductivity and viscosity of nanofluids containing carbon nanotubes. *Nanoscale Res. Lett.* **2014**, *9*, 151. [[CrossRef](#)]
38. Nabil, M.; Azmi, W.; Hamid, K.A.; Zawawi, N.; Priyandoko, G.; Mamat, R. Thermo-physical properties of hybrid nanofluids and hybrid nanolubricants: A comprehensive review on performance. *Int. Commun. Heat Mass Transf.* **2017**, *83*, 30–39. [[CrossRef](#)]
39. Daviran, S.; Kasaeian, A.; Tahmooressi, H. Evaluation of clustering role versus brownian motion effect on the heat conduction in nanofluids: A novel approach. *Int. J. Heat Mass Transf.* **2017**, *108*, 822–829. [[CrossRef](#)]
40. Song, D.; Hatami, M.; Wang, Y.; Jing, D.; Yang, Y. Prediction of hydrodynamic and optical properties of TiO₂/water suspension considering particle size distribution. *Int. J. Heat Mass Transf.* **2016**, *92*, 864–876. [[CrossRef](#)]
41. Lin, J.; Cai, X.; Liu, Z.; Liu, N.; Xie, M.; Zhou, B.; Wang, H.; Guo, Z. Anti-liquid-interfering and bacterially antiadhesive strategy for highly stretchable and ultrasensitive strain sensors based on cassie-baxter wetting state. *Adv. Funct. Mater.* **2020**, *30*, 2000398. [[CrossRef](#)]